Available online at www.sciencedirect.com
ScienceDirect
Journal of Photochemistry and Photobiology A: Chemistry 193 (2008) 33–41
Journal of Photochemistry and Photobiology A:Chemistry
www.elsevier.com/locate/jphotochem

Two-step synthesis of a novel visible-light-driven $K_2Ta_2O_{6-x}N_x$ catalyst for the pollutant decomposition

Shengbao Zhu [a], Hongbo Fu [a,b,*], Shicheng Zhang [a,b], Liwu Zhang [a], Yongfa Zhu [a,**]

[a] *Department of Chemistry, Tsinghua University, Beijing 100084, China*
[b] *Department of Environmental Science & Engineering, Fudan University, Shanghai 200433, China*

Received 7 September 2006; received in revised form 16 May 2007; accepted 7 June 2007
Available online 13 June 2007

Abstract

Visible-light-driven $K_2Ta_2O_{6-x}N_x$ catalysts have been synthesized successfully from N-doped Ta_2O_5 precursors in KOH solutions by a simple hydrothermal process. $K_2Ta_2O_{6-x}N_x$ with pyrocrhore structure could be obtained at above 160 °C for 24 h. $K_2Ta_2O_{6-x}N_x$ crystals presented cube-shaped morphologies, and absorbed the visible-light up to the wavelength of 600 nm. The as-prepared sample could decompose formaldehyde efficiently under the visible irradiation ($\lambda > 400$ nm), and its photocatalytic activity depended on the N-doping content and the hydrothermal temperature. $K_2Ta_2O_{5.982}N_{0.018}$ prepared at 220 °C for 24 h showed the highest photoactivity for the formaldehyde degradation. Additionally, it presented much higher activity than that of the sample prepared by the NH_3 annealing directly. The visible-light response of $K_2Ta_2O_{6-x}N_x$ catalyst could be closely related to the N-doping content. As the x values were >0.256, the valence-band of the catalyst was composed of the hybrid O 2p and N 2p orbitals, and the visible-light sensitivity was due to the narrowing of the band-gap by mixing the N 2p and O 2p states. However, as the x values were <0.073, the isolated narrow band formed above the valence-band of O 2p was responsible for the visible-light response.

Keywords: Photocatalytic; N-doping; $K_2Ta_2O_6$; Two-step synthesis; Hydrothermal process; Formaldehyde

1. Introduction

Photocatalysis are currently applied to solve the energy problems and to meet the demand of environmental clean-up [1–3]. Heterogeneous photocatalysis offer great potential for converting photon energy into chemical energy and for decomposing pollutants in air or solution [4–6]. Recently, It has been discovered high photocatalytic activities in some alkaline and alkaline earth tantalates, including $NaTaO_3$ [7–9], $KTaO_3$ [10–12], $LiTaO_3$ [13], $SrTa_2O_6$ [14], $BaTa_2O_6$ [7], and $Sr_2Ta_2O_7$ [15]. However, most of these tantalum oxides have the band-gap energies that are too large to use solar radiation efficiently. In these Ta^{5+}-based oxides, the valence-bands predominantly consist of O 2p orbitals whose levels of the potential energy are located at a deep position of about 3.0 eV versus NHE (or about −7.44 eV versus vacuum level). Due to this fact, it is not feasible to find a transition metal oxide that functions under the visible-light irradiation. Although NiO-modified $InTaO_4$ was reported recently as an effective photocatalyst for water-splitting under the visible-light irradiation, the absorption in the visible-light region was not significant, and the photocatalytic efficiency was very low [16].

Recently, (oxy)nitrides containing Ta^{5+} and Ti^{4+}, such as Ta_3N_5 [17], TaON [18], $Ta_2O_{5-x}N_x$ [19], and $TiO_{2-x}N_x$ [20–26] were also found to have the potential activity for water-splitting or decomposition of pollutants under the visible-light irradiation. These materials could be synthesized by nitriding the corresponding metal oxides under NH_3, and absorb the visible-light up to the wavelength of 600 nm. It is understood that the partial replacement of O^{-2} by N^{-3} narrows the band-gap of the parent oxides by shifting their valence-band upward. The changes in the resulting optical properties of these materials have fueled a number of the recent studies [17–26]. It is widely recognized that the N dopants may be more appropriate to extend the photocatalytic activity to the visible-light region because the related impurity states are supposed to be close to the valence-band maximum. Density function theory calculations for $TiO_{2-x}N_x$, TaON, and Ta_3N_5 have revealed these materials

* Corresponding author at: Department of Chemistry, Tsinghua University, Beijing 100084, China. Tel.: +86 10 6278 7601; fax: +86 10 6278 7601.
** Corresponding author. Tel.: +86 10 6278 7601; fax: +86 10 6278 7601.
E-mail addresses: fuhb@fudan.edu.cn (H. Fu), zhuyf@mail.tsinghua.edu.cn (Y. Zhu).

1010-6030/$ – see front matter © 2007 Published by Elsevier B.V.
doi:10.1016/j.jphotochem.2007.06.004

to have the following common features. The formal electronic configurations of transition metal cations are d^0, the bottoms of the conduction bands consist of empty d orbitals, and the tops of the valence-bands mainly consist of the N 2p orbitals or the hybrid O 2p and N 2p orbitals, resulting in the smaller band-gap energies than the pure oxides [20,27].

In our previous report, $K_2Ta_2O_6$ crystal with pyrocrhore structure showed high photocatalytic activity for the RhB decomposition under the UV light irradiation [28]. Very recently, Takita and coworkers also reported that the pyrocrhore $K_2Ta_2O_6$ showed much higher activity for water-splitting than that of $KTaO_3$ catalyst with perovskite structure [29]. Accordingly, it is expected that N-doped $K_2Ta_2O_6$ prepared via suitable route is active under the visible-light irradiation, as other nitrogen-containing Ta^{5+}-based materials.

The preparation of nitrogen-containing tantalum oxide is synthesized conventionally by a high-temperature reaction of nitrogen, ammonia, or the hydrogen/nitrogen mixture with the metal or its oxide, typically at the temperature of around 1000 °C over long periods [17–19]. Problems associated with the preparation include the unreacted metal in the product, and lack of control over the crystallinity and the particle size. Especially, a drastic growth of the resulting nitride particles occur inevitably on the surface of the oxides during this process, resulting in a decrease in the photocatalytic activity [17]. Furthermore, as for some compound such as Bi_2WO_6, it is difficult to dope N into the crystal lattice of the catalyst by a NH_3 annealing directly due to the reductive function of NH_3. Considering the need to obtain a pure and homogeneous sample with a high surface area for catalytic applications, solution processing is expected to be satisfactory. We have developed a hydrothermal method previously, which was applied successfully to prepare the photocatalysts with the enhanced activities for the pollutant decompositions as compared to the samples prepared by a solid-state reaction at high temperatures [30,31].

In this report, $K_2Ta_2O_{6-x}N_x$ photocatalyst was prepared successfully by a two-step synthesized route. To introduce N dopants, N-doped Ta_2O_5 was synthesized first by annealing a commercial Ta_2O_5 in a NH_3 flow at 750 °C. $K_2Ta_2O_{6-x}N_x$ catalyst was then gained using N-doped Ta_2O_5 as a starting material in KOH solution by the hydrothermal process. The as-prepared samples were characterized by X-ray photoelectron spectroscopy (XPS), X-ray diffraction (XRD), and UV–vis diffuse reflection (DR) spectroscopy. The formaldehyde (FAD) decomposition was used to be a probe reaction to evaluate the photoactivity of the catalyst. To the best of our knowledge, such synthesis for visible-light-driven photocatalysts was never designed, and this method was suitable particularly to some mixing oxide that could not be modified by the NH_3 annealing directly at the high temperature.

2. Experimental

2.1. Preparation of $K_2Ta_2O_{6-x}N_x$ catalysts

N-doped Ta_2O_5 was synthesized according to the previous report [19]. Commercial Ta_2O_5 (99.99%) was treated in a flow reactor in a N_2 gas atmosphere (1 atm) at 750 °C. Typical heating rates were 7 °C min^{-1}. For doping, N_2 flow was replaced by NH_3 for 10–60 min after the target temperature was reached. Subsequently, the crystals were cooled in flowing N_2. N-doped Ta_2O_5 was then chosen as the starting materials in KOH solution for the hydrothermal synthesis of $K_2Ta_2O_{6-x}N_x$. In a typical synthesis procedure, 1.68 g of KOH (30 mM) and 0.442 g of N-doped Ta_2O_5 (1 mM) were added to 30 mL of deionized water with magnetic stirring. A series of the mixtures were sealed in a Teflon-lined stainless steel autoclave, and heated in the range of 100–240 °C under an autogenous pressure for 24 h. After cooling, the resulting product was filtered, washed, and dried at ambient temperature. For comparison, N-doped $K_2Ta_2O_6$ sample was prepared by the NH_3 annealing directly from a hydrothermal $K_2Ta_2O_6$ sample. The chemicals were all of analytical grades, and were used without further purification. Deionized water was used throughout this study.

2.2. Characterization

Morphologies and microstructures of the as-prepared samples have been determined using a JEOL JEM 1010 TEM operated at an accelerating voltage of 120 kV. High-resolution TEM (HRTEM) images were obtained with a JEM 2010F field emission gun transmission electron microscope operated at an accelerating voltage of 200 kV. The samples were prepared by dispersing the powders in water, and depositing a drop of suspension onto a thin Formavar film supported on a Cu grid. The specific surface areas were determined by a Flow Sorb 2300 apparatus (Micromeritics) with a single-point BET method. XRD patterns of the powders were recorded using a Bruker D8 Advance X-ray diffractometer with a Cu Kα radiation at a 2θ scan rate of 2° min^{-1}. XPS analysis was measured on a PHI 5300 ESCA instrument using an Al Ka X-ray source at a power of 250 W. The pass energy of the analyzer was set at 35.75 eV, and the base pressure of the analysis chamber was $<3 \times 10^{-9}$ Torr. The binding energy scale was calibrated with respect to the C 1s peak of hydrocarbon contamination fixed at 285.0 eV. It was reported that the peak at around 396 eV corresponds to N 1s, derived from Ta–N bonds [19,21]. Because the peak area of N 1s was overlapped partly with that of Ta $4p_{3/2}$, a method of the peak separation was applied to calculate the peak area of N 1s. Therefore, the x values (nitrogen concentrations) were estimated by comparing the product of the 396 eV peak area multiplied by a nitrogen-sensitive factor to the product of the peak area at 531 eV (O 1s, Ta–O bonds) multiplied by a oxygen-sensitive factor [20,21]. UV–vis DR spectra were obtained with a Hitachi U-3010 spectrometer (Japan). $BaSO_4$ was the reference sample, and the spectra were recorded in the range of 200–700 nm.

2.3. Photoreactor and light source

The photocatalytic activities were evaluated by the decomposition of FAD under the visible-light ($\lambda > 400$ nm) irradiation. A 500 W Xenon lamp (the Institute of Electric Light Source, Bei-

jing) was focused through a window, and a 400 nm cutoff filter was placed onto the window face of the cell to ensure the desired irradiation. The average light intensity was 40 mW cm^{-2}. The irradiation area was approximately 40 cm^2. The radiant flux was measured with a power meter (the Institute of Electric Light Source, Beijing).

2.4. Procedure and analyses

The sample was spread evenly and uniformly without open spaces in the sample over the irradiation area (approximately 9.4 cm^2) in 250 mL of the vessel. In this experimental condition, irradiated light was absorbed only on the outer geometric surface of the powder. Certain concentration of the reactant gas was injected into the vessel, and then the samples were stored in the dark. The irradiation started when the gas concentration was constant. The amounts of FAD were determined using a gas chromatograph (SP-502) with FID.

3. Results and discussion

3.1. Structural characterization

To determine an optimum hydrothermal temperature for $K_2Ta_2O_{6-x}N_x$ to be well-crystallized, the precursor (N-doped Ta_2O_5) for $K_2Ta_2O_{6-x}N_x$ synthesis was treated in KOH solution in the range 100–240 °C for 24 h. XRD patterns of the as-prepared samples are shown in Fig. 1. In the spectrum (a), all of the reflections could be readily indexed as the orthorhombic Ta_2O_5 (JPCDS 25-0922). Neither TaON nor Ta_3N_5 phases were observed [19]. It was clearly seen that a partial crystallization of $K_2Ta_2O_6$ occurred at 100 °C, and $K_2Ta_2O_6$ with single pyrochlore phase was completed at above 160 °C (Fig. 1e). In the spectrum (e), all of the reflections could be readily indexed as pyrochlore $K_2Ta_2O_6$ [space group: 2 2 7] identical to the JCPDS card (35-1464), which was also consistent with the data reported by our group previously [28]. In the scope of 160–220 °C, XRD patterns of the samples were similar. However, the intensities of the diffraction peaks decreased apparently when the sample was treated at 240 °C, suggesting that the qualities of the crystallines decreased.

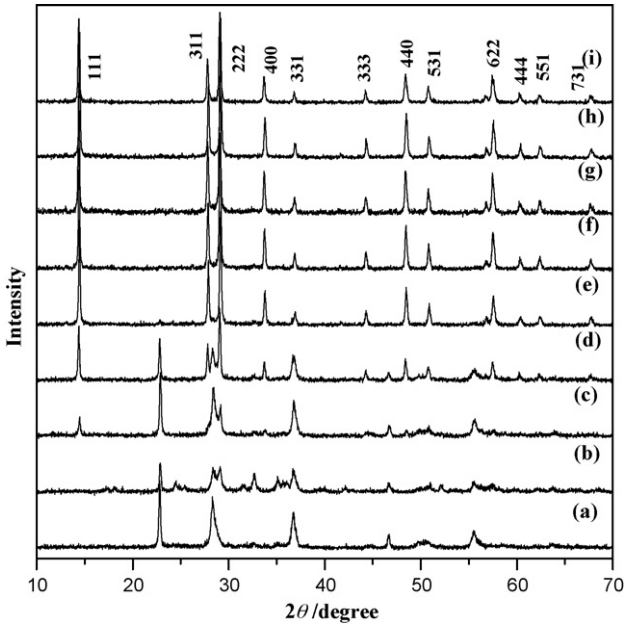

Fig. 1. XRD patterns of the samples prepared at the different hydrothermal temperatures: the precursor (a), 100 °C (b), 120 °C (c), 140 °C (d), 160 °C (e), 180 °C (f), 200 °C (g), 220 °C (h), and 240 °C (i).

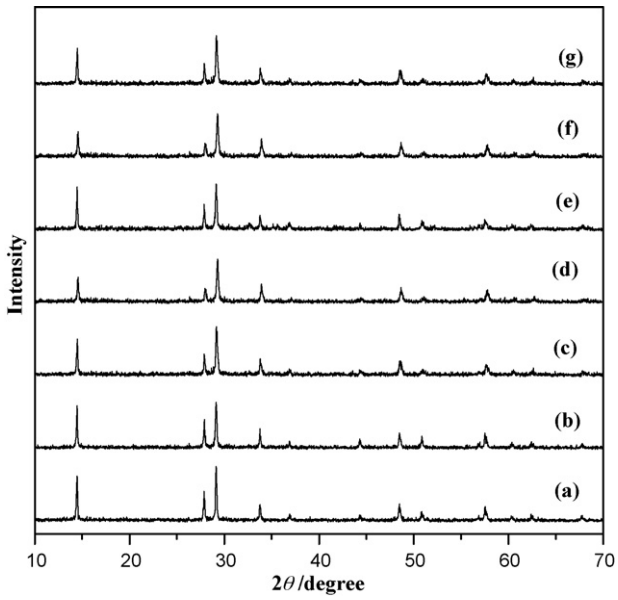

Fig. 2. XRD patterns of the samples prepared at 220 °C from N-doped Ta_2O_5 with the different annealing times: 0 min (a), 10 min (b), 20 min (c), 30 min (d), 40 min (e), 50 min (f), and 60 min (g).

To probe the effect of the N-doped content on the crystal, Ta_2O_5 with the different N-doped content were selected as the precursors for $K_2Ta_2O_{6-x}N_x$ synthesis at 220 °C for 24 h. XRD patterns of the as-prepared samples are shown in Fig. 2. Replacing an O atom with an N atom in the products did not result in significant structural changes. This could be understood that the concentration of N-doping (given later) might be low, although it held a larger ion radius of 0.171 nm than 0.132 nm of an O atom.

3.2. Morphologies of the catalysts

The morphologies and microstructures of the as-prepared samples were then investigated with TEM. As is shown in Fig. 3, it could be seen that the morphologies and dimensions of the samples were dependent strongly on the hydrothermal temperature. Fig. 3a shows the TEM micrograph of the starting precursor. The starting precipitates were irregular in shape. When the sample was treated at 100 °C, the morphology of the sample was similar to that of the precursor, but the smaller size. For 120 °C, the sample was still irregular, but some cubic structure produced among the formless particles. With the increase of the temperature to 140 °C, the mixture of granule- and cube-shaped crystals were present (Fig. 3d), suggesting that a large quantity of tiny crystalline nuclei were still in existence. At this point, selective area electron diffraction (SAED) experiment shown in the corner

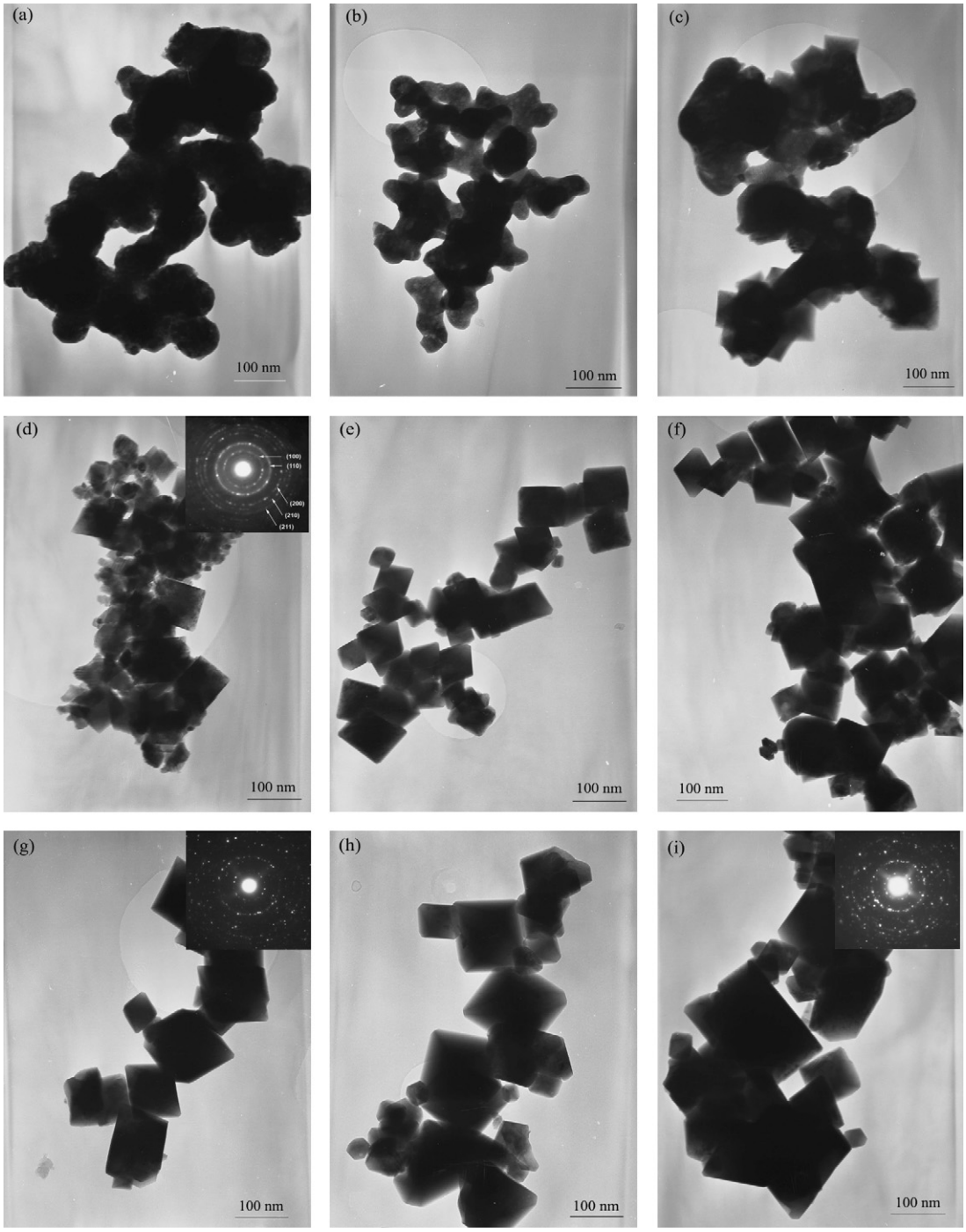

Fig. 3. TEM images of the samples prepared by the hydrothermal process at the different temperatures: the precursor (a), 100 °C (b), 120 °C (c), 140 °C (d), 160 °C (e), 180 °C (f), 200 °C (g), 220 °C (h), and 240 °C (i).

of Fig. 3d also confirmed that many polycrystalline particles were available. For 160 °C, the crystal was cube-like basically in shape, and the crystallite size was several decade nanometers. When the temperature further rose to 200 °C, the cube-shaped crystal grew larger, and the edges of the most crystals in length were about 100 nm. However, SAED experiment showed an unclear polycrystalline ring, suggesting that a small quantity of tiny crystalline nuclei still existed. When the sample was treated at the higher temperature, such as 240 °C, the size of the crystal grew larger, and the morphologies of the crystals became heterogenerous. This phenomenon was especially notable when the sample was prepared at 240 °C (Fig. 3i). The samples held the large primary cubes and the smaller secondary ones, which could originate from the breakage of the large one. The pattern in the corner of Fig. 3i showed a clearer polycrystalline ring compared to the one in the corner of Fig. 3g, indicating the destruction of the matured cube-shaped crystals under the harsh condition.

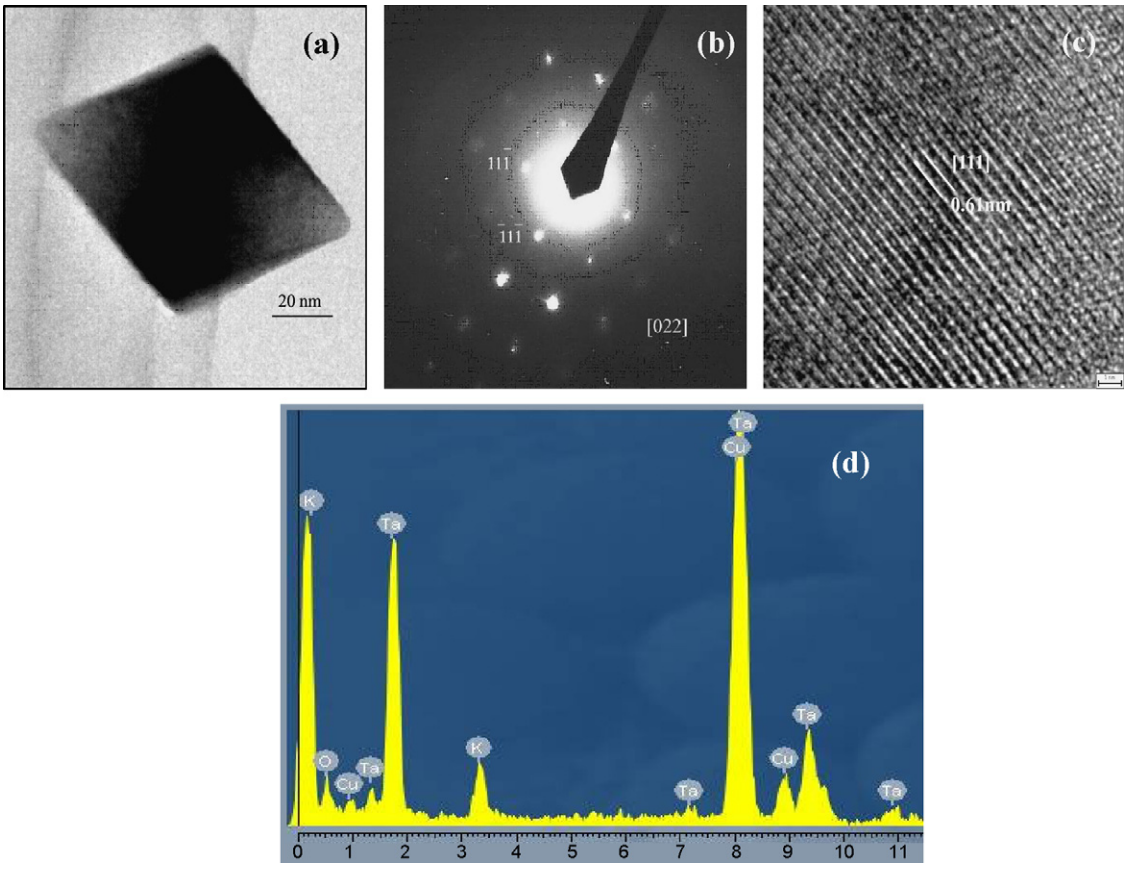

Fig. 4. Typical $K_2Ta_2O_{5.936}N_{0.064}$ nanocube prepared at 200 °C for 24 h: the amplified TEM (a), ED pattern (b), HRTEM image (c), and EDAX spectrum (d).

3.3. Formation mechanism of $K_2Ta_2O_{6-x}N_x$ nanocube

As is shown in Fig. 4a, a typical TEM image of the sample prepared at 200 °C for 24 h presented clearly a perfect cube-like morphology with the edges about 100 nm in length. The indexed (0 2 2) zone electron diffraction pattern (Fig. 4b) originated from a single nanocube (Fig. 4a) revealed a single-crystalline nature of the nanocube. HRTEM image (Fig. 4c) shows that the nanocube with perfect edges is uniform structurally with an interplanar spacing of about 0.61 nm, corresponding to the (1 1 1) lattice spacing of $K_2Ta_2O_{6-x}N_x$. Lattice defects induced by N-doping could not be observed from the HRTEM image. Energy dispersive analysis of X-rays (EDAX) was performed for the element constituents of the nanocube, which is shown in Fig. 4d. Only Ta, K, and O element were found in the spectrum except for Cu element brought by the Cu grid. Quantitative results gave the atomic ratio of 1:1.15 for K:Ta, which was close to the ideal value of 1.

The hydrothermal process with amorphous nanoparticles as precursors is a typical Oswald ripening process [30–34]. In the current work, a highly supersaturated KOH solution was adopted, and an amorphous inorganic material of N-doped Ta_2O_5 was selected as precursors. The tiny crystalline nuclei engendered first, and then followed by crystal growth. The larger cubes would grow at the expense of the small ones because of the difference between the large crystal and the smaller one of a higher solubility on the basis of the well-known Gibbs–Thomson law [33]. TEM images showed the coexistence of the small cubes and the irregular nanoparticles when the sample was prepared at 140 °C (Fig. 4d). With the increase of the temperature, the irregular nanoparticles disappeared, and larger irregular cubes occurred, indicating that the larger crystals grew at the expense of the smaller ones. The high-quality nanocubes formed only at the feasible treatment temperature (200 °C). Over the higher-temperature treatment led to the breakage of matured nanocubes, and reduced their quality, which could be observed from the TEM images and XRD results.

3.4. N content in the catalysts

XPS technique was employed to probe the N-doped content of the as-prepared samples. Global XPS profiles for the samples synthesized at above 160 °C are shown in Fig. 5A. According to the XPS spectra, the samples contained Ta, O, K, and N atoms. And binding energies for Ta 4s, O 1s, N 1s & Ta 4p, K 2s, C 1s, K 2p, and Ta 4d are 573, 523, 395–405, 380, 292, 285, and 234 eV, respectively. Fig. 5B shows N 1s spectra of the as-prepared samples. A new peak in the region of 395–396 eV was observed, which was considered generally as the evidence for the presence of Ta–N bonds, suggesting that the oxygen atoms were substituted successfully by the nitrogen atoms [19]. Considering XRD patterns and XPS spectra, the powders prepared at above 160 °C were described as $K_2Ta_2O_{6-x}N_x$. As the hydrothermal temperature increased, the peak around 396 eV decreased in intensity,

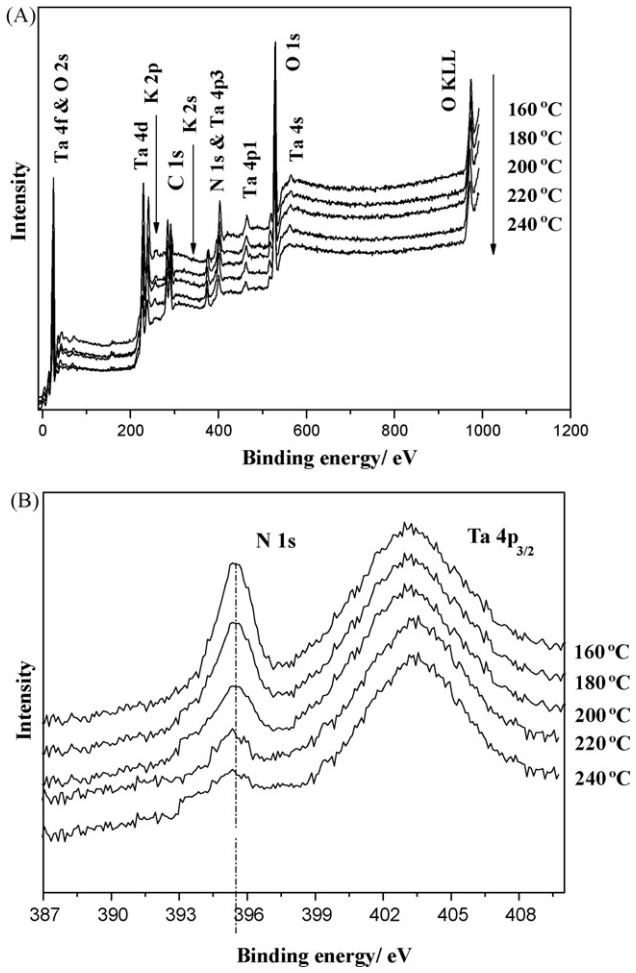

Fig. 5. Global XPS of the samples prepared at above 160 °C (A), and the N 1s peak around the 396 eV regions (B).

which could be because that the adventitious N_2, NH_3, or N-containing organic compounds adsorbed on the surface of the precursor escaped off when the sample was treated during the hydrothermal process [25]. N 1s spectra of the sample prepared from Ta_2O_5 precursors with the different N-doping content were also observed (not shown). The profile of the spectra was similar with those in Fig. 5B. A new peak also appeared at 395–396. As N-doped Ta_2O_5 with higher N-doping content was selected as a precursor, the resulting product contained higher N content, accordingly. The sample prepared from N_2 gas annealed did not display a peak at 396 eV. The estimated x values in $K_2Ta_2O_{6-x}N_x$ from the XPS spectra are listed in Tables 1 and 2, respectively.

Table 2
x and k values of the $K_2Ta_2O_{6-x}N_x$ catalysts prepared at 220 °C from N-doped Ta_2O_5 precursors with the different NH_3 annealing times

Annealing time (min)	x in $K_2Ta_2O_{6-x}N_x$	k (h^{-1})
Air 60	0	–
NH_3 10	0.018	0.254
NH_3 20	0.052	0.153
NH_3 30	0.073	0.089
NH_3 40	0.256	0.048
NH_3 50	0.348	0.029
NH_3 60	0.453	0.019

3.5. Optical properties of the catalysts

Fig. 6A shows DR spectra of the samples prepared at different hydrothermal temperatures. N-doped Ta_2O_5 precursor obviously absorbed the visible-light (>400 nm). The absorption of the as-prepared sample in the visible region decreased with increasing hydrothermal temperature, which was in accordance with the XPS results. $K_2Ta_2O_{6-x}N_x$ samples prepared at above 160 °C showed almost the same absorption onsets. However, the mixtures of $K_2Ta_2O_{6-x}N_x$ and N-doped Ta_2O_5 prepared at below 160 °C presented the different onsets. With the increase of the hydrothermal temperature, the absorbance onset of the resulting sample shifted apparently toward the short wavelength.

Fig. 6B shows DR spectra of the samples prepared from the Ta_2O_5 precursors with the different N-doped contents treated at 220 °C for 24 h. The as-prepared powders absorbed the visible-light. This absorption in the region of 400–600 nm was related to the presence of nitrogen because it increased with the content of N-doping. Additionally, the absorption edge well agreed with the reported value for the N-doped Ta_2O_5 [19]. It was noteworthy that the onsets of the catalysts were dependent strongly on the x values in $K_2Ta_2O_{6-x}N_x$. When the x values were <0.073, the samples showed the same absorption onsets, and the shoulders in the visible-light region increased. However, when the x values were >0.256, the absorption onsets of the samples were red-shift apparently. The absorption in the visible region increased greatly. The inset of Fig. 6B shows the amplified DR spectra of the samples ($x = 0$ and 0.018) in wavelength of about 400 nm. One can see that the sample ($x = 0.018$) present an insignificant absorbance. However, the sample ($x = 0$) have no a visible absorbance.

For a crystalline semiconductor, it was shown that the optical absorption near the band-edge follows the equation: $ahv = A(hv - E_g)^{n/2}$, where a, v, E_g, and A are absorption coefficient, light frequency, band-gap, and a constant, respectively. The values of n and E_g were determined by the following steps: first, plot

Table 1
Surface area, x values, and k values for the $K_2Ta_2O_{6-x}N_x$ catalysts prepared at the different temperature under the NH_3 flow for 20 min

	Sample									
	$Ta_2O_{5-x}N_x$ (precursor)	100 °C	120 °C	140 °C	160 °C	180 °C	200 °C	220 °C	240 °C	$K_2Ta_2O_6$ (220 °C)
Surface area ($m^2\ g^{-1}$)	–	12.6	12.4	10.4	9.4	9.5	7.7	8.3	8.0	6.7
x value	–	–	–	–	0.079	0.066	0.064	0.052	0.035	–
k (h^{-1})	0.028	0.029	0.038	0.043	0.078	0.092	0.100	0.153	0.170	–

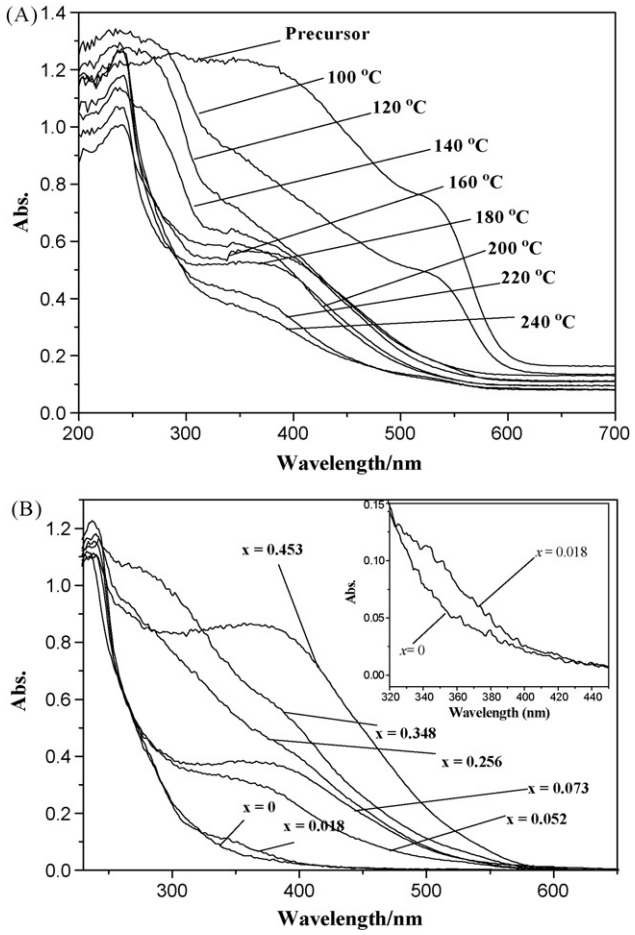

Fig. 6. DR spectra of the samples prepared at the different temperatures (A), and the samples prepared at 220 °C with the different N contents (B). The amplified DR spectra of the samples ($x = 0$ and 0.018) in wavelength of around 400 nm (inset of (B)).

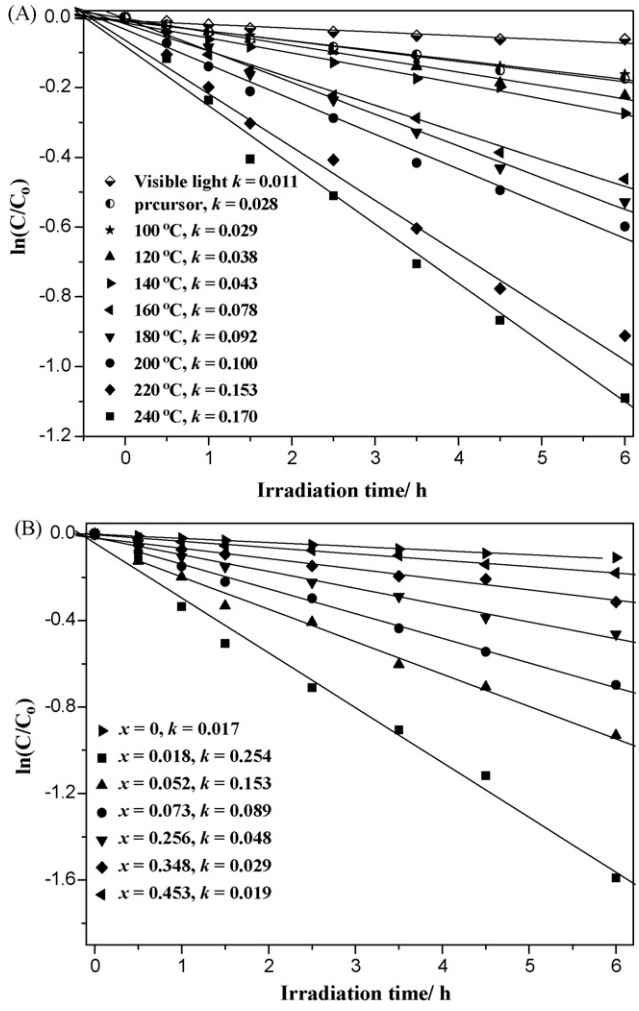

Fig. 7. The influence of the hydrothermal temperature (A) and N-doping content (B) on the photoactivites of the samples for the FAD photodegradation. FAD concentration, 1387 ppm; catalyst loading, 0.3 g L^{-1}, $\lambda > 400$ nm.

$\ln(ahv)$ versus $\ln(hv - E_g)$, using an approximate value of E_g, and then determine the value of n with the slope of the straightest line near the band edge; second, plot $(adv)^{2n}$ versus hv and then evaluate the band gap E_g by extrapolating the straightest line to the hv axis intercept [35]. According to the equation, the value of n for $K_2Ta_2O_6$ was 2 from the data in Fig. 6B. The band-gaps of $K_2Ta_2O_6$ and $K_2Ta_2O_{6-x}N_x$ ($x < 0.073$) were estimated to be 4.43 eV from the onset of the absorption edge. The band-gaps of the samples with the x values of 0.256, 0.348, and 0.453 were estimated to be 2.43, 2.31, and 2.25 eV, respectively. These crystals in color varied from pale-yellow to dark-red, and the color was darker gradually as x increase. Whereas, the undoped $K_2Ta_2O_6$ sample was colorless. The presence of the visible absorption indicated that nitrogen penetrated into the single crystal, and changed the electronic structure of the crystal effectively [19,23].

3.6. Photocatalytic activity

To evluate the photocatalytic activities of the as-prepared samples, the photodegradation of FAD was investigated under the visible-light irradiation. Fig. 7A shows the degradation of FAD over the samples prepared at different temperatures. The first-order linear relationship was revealed by the plots of $\ln(C/C_0)$ versus time (t). In this system, it can be explained in a Langmuir–Hinshelwood model. When solution is dilute, the reaction rate can be expressed by

$$r = kKC \quad (1)$$

K refers to the adsorption equilibrium constant, k the reaction constant, and C is the concentration of the reactant. Formaldehyde could not be degraded by the visible-light. With the increase of the hydrothermal temperature, the sample showed higher photoactivity for the FAD degradation. The sample prepared at 240 °C showed the highest activity, and the results are shown in Table 1. The effect of N-doping content on the photoactivity of the as-prepared sample was also observed, and the results are shown in Fig. 7B and Table 2. Irradiating the undoped sample with the visible-light did not generate the decrease of FAD because $K_2Ta_2O_6$ was not visible-light sensitive. However, the degradation of FAD was observed from all the other samples, suggesting that N-doping was an effective and feasible approach for achieving the visible-light-driven photocatalysts.

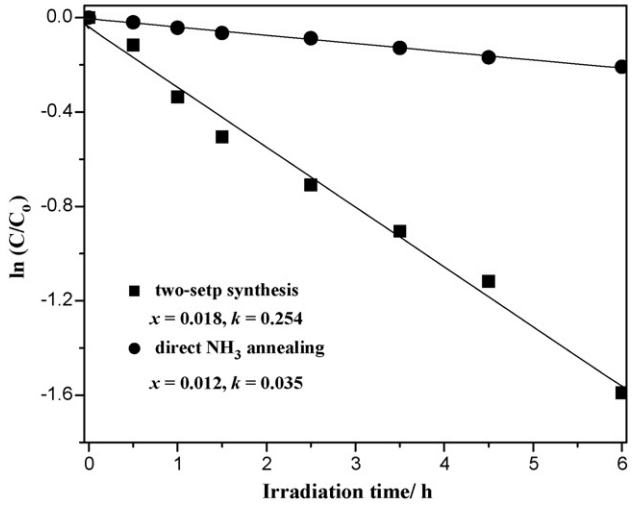

Fig. 8. Photocatalytic degradation of FAD over the catalysts prepared by the different methods under the visible-light irradiation. Photocatalyst, 0.3 g; FAD concentration, 1387 ppm in air; $\lambda > 400$ nm.

As the x values increased, the photoactivies of the samples decreased, which was similar to that of N-doped TiO_2 or Ta_2O_5 [19,21]. $K_2Ta_2O_{5.982}N_{0.018}$ catalyst showed the highest activity for the FAD photodegradation among all the samples, though it shows an insignificant adsorption in the visible region (>400 nm) (shown in the inset of Fig. 6B).

The FAD photodegradation over N-doped $K_2Ta_2O_6$ samples prepared by the different methods was performed, and the result is shown in Fig. 8. The as-prepared sample showed higher photoactivity for the FAD degradation than that of the sample prepared by the NH_3 annealing directly. The reaction constant (k) of the sample prepared by the two-step synthesis is higher by about seven times than that of the sample prepared by the NH_3 annealing, indicating that much higher photocatalytic activities of the as-prepared sample performed under the visible-light irradiation. When the sample is prepared directly at the high temperature, it is difficult to control over the crystallinities and particle sizes of the samples. Especially, the exaggeration of the resulting nitride particles occurs inevitably during the high-temperature process, resulting in a decrease in the photocatalytic activity.

Many factors, e.g., surface area, crystallinity, and oxygen vacancy affect the activity of a photocatalyst [36]. The surface areas of the samples prepared at the different temperatures are shown in Table 1. The samples prepared at below 160 °C showed relatively small activities ($k < 0.043\ h^{-1}$) despite of their large surface areas (10.4–12.6 $m^2\ g^{-1}$). The activity of the sample for the FAD photodegradation increased rapidly from $k = 0.029$ to $0.10\ h^{-1}$, while the corresponding surface area decreased moderately from 12.6 to 7.7 $m^2\ g^{-1}$. There are two conflicting factors that affect the overall photocatalytic activity in an opposite way (i.e., the number of lattice defects and the surface area). Lattice defects may act as the recombination centers for the photoinduced electrons and holes, thus reducing significantly the net photocatalytic activity [36,37]. The decrease in the photocatalytic activity of the sample prepared at the lower temperature may therefore be understood in such a way, namely, that the abundant lattice defects acting as inactivation centers increased due to its poor crystallinity, which could be observed from the XRD and TEM results. Especially, XRD patterns reveal that the sample prepared at below 160 °C still contains the notable impurity of Ta_2O_5. The defects induced by non-stoichiometry can also be an additional reason for decreasing drastically the photocatalytic activity. It is worthy noting that the lattice defects in the catalysts could be originated from two ways. One is from the uncompleted hydrothermal reaction, and the other occurs by N-doping from the precursor. It is well known that N dopants act as a recombination center of the photogenerated charge carriers, and thus deteriorate the photoactivity of the catalyst [21]. Therefore, the sample prepared at 240 °C showed the highest photoactivity due to the lower N-doped content, although it held the worse crystal phase than the sample prepared at 200 °C.

3.7. Visible-light-induced photocatalysis

In the present study, the band structure of $K_2Ta_2O_{6-x}N_x$ was dependent strongly on N-doping content. UV–vis spectra in Fig. 6 indicated that the absorption edges of the catalysts were not affected by the N-doping when the x value is <0.073. As the x value increased from 0.256, N-doping caused the narrowing of the band gap of the catalysts. It is plausible that the band structure of $K_2Ta_2O_{6-x}N_x$ with lower values of x (<0.073) should be different from those with higher x values (>0.256). Our results are in good agreement with the previous report [20,21]. Accordingly, it was concluded that the isolated narrow band formed above the valence-band is responsible for the visible-light response when N-doping content is low in the catalyst (<0.073). However, in the high N-doping content (>0.256), the hybrid orbitals of O 2p and N 2p could be responsible for the visible-light absorption. On the basis of this hypothesis, irradiation with visible-light excites electrons in the hybrid O 2p and N 2p orbitals in the catalysts with high N-doping content. As for the catalysts with the low N-doping content, irradiating with visible-light only excites electrons in N induced mid-gap.

Transfer of charge carries is a vital factor to influence on the photoactivity of the catalyst. When a photon is absorbed by $K_2Ta_2O_{6-x}N_x$, an e^-/h^+ pair is generated. The e^- and h^+ could migrate to the surface to react with the adsorbed FAD in the desired process, or then could undergo a non-desired recombination. N-doping caused an increase in oxygen vacancy which acts as a recombination center for holes and electrons [21]. As N-doped Ta_2O_5 with the higher N-doping content was used as a precursor for the synthesis, the more oxygen vacancies occur in the resulting products, which could explain why the activity of the powder were lower as x increased.

4. Conclusions

Visible-light-driven $K_2Ta_2O_{6-x}N_x$ catalysts have been prepared by a two-step synthesis. First, N-doped Ta_2O_5 was annealed under an NH_3 flow at 750 °C. Then, $K_2Ta_2O_{6-x}N_x$ was synthesis using N-doped Ta_2O_5 as a starting material. The single-phase $K_2Ta_2O_{6-x}N_x$ crystals were cube-shaped when the

temperature was settled at above 160 °C for 24 h, and the as-prepared samples showed nitrogen substituted at some of the oxygen sites in the resulting product. The samples showed the photoactivities for the decomposition of FAD under the visible-light irradiation. The activity of the sample decreased with the increase of N-doping concentration. $K_2Ta_2O_{5.982}N_{0.018}$ prepared at 220 °C for 24 h showed the highest photoactivity for the FAD degradation, and it also displayed much higher activity than the sample prepared by the NH_3 annealing directly.

In conclusion, this study showed a novel approach to synthesis N-doped oxide. Such material could efficiently utilize the visible-light for the pollutant photodegradation. Further study about the two-step synthesis of N-doped $NaTaO_3$ for water-splitting is in progress.

Acknowledgments

This work was supported partly by the Chinese National Science Foundation (20433010, 20571047) and Trans-Century Training Program Foundation for the Talents by the Ministry of Education, PR China, and China Postdoctoral Science Foundation (2005037050).

References

[1] M.R. Hoffmann, S.T. Martin, W. Choi, Chem. Rev. 95 (1995) 69.
[2] A. Fujishima, K. Honda, Nature 238 (1972) 37.
[3] H. Fu, X. Quan, Z. Liu, S. Chen, Langmuir 20 (2004) 4867.
[4] E. Bae, W. Choi, Environ. Sci. Technol. 37 (2003) 147.
[5] S. Kim, W. Choi, Environ. Sci. Technol. 36 (2002) 2019.
[6] Y.M. Xu, C.H. Langfor, Langmuir 17 (2001) 897.
[7] H. Kato, A. Kudo, J. Phys. Chem. B 105 (2001) 4285.
[8] H. Kato, A. Kudo, Catal. Lett. 58 (1999) 153.
[9] H. Kato, K. Asakura, A. Kudo, J. Am. Chem. Soc. 125 (2003) 3082.
[10] T. Ishihara, H. Nishiguchi, K. Fukamachi, Y. Takita, J. Phys. Chem. B 103 (1999) 1.
[11] K. Sayama, H. Arakawa, K. Domen, Catal. Today 28 (1996) 175.
[12] V. Laguta, M.D. Glinchuk, I.P. Bykov, A. Gremona, P. Galinetto, E. Giulotto, L. Jastrabik, J. Rosa, J. Appl. Phys. 93 (2003) 6056.
[13] H. Kato, A. Kudo, Chem. Phys. Lett. 295 (1998) 487.
[14] H. Kato, A. Kudo, Chem. Lett. (1999) 1207.
[15] A. Kudo, H. Okutomi, S. Nakagawa, J. Phys. Chem. B 104 (2000) 571.
[16] G. Hitoki, T. Takata, J. Kondo, M. Hara, H. Kobayashi, K. Domen, Chem. Commun. (2002) 1698.
[17] Q. Zhang, L. Gao, Langmuir 20 (2004) 9821.
[18] D. Lu, G. Hitoki, E. Katou, J. Kondo, M. Hara, K. Domen, Chem. Mater. 16 (2004) 1603.
[19] T. Murase, H. Irie, K. Hashimoto, J. Phys. Chem. B 108 (2004) 15803.
[20] R. Asahi, T. Morikawa, K. Aoki, Y. Taga, Science 293 (2001) 269.
[21] H. Irie, Y. Watanabe, K. Hashimoto, J. Phys. Chem. B 107 (2003) 5483.
[22] M. Mrowetz, W. Balcerski, A.J. Colussi, M.R. Hoffmann, J. Phys. Chem. B 108 (2004) 17270.
[23] C.D. Valentin, G. Pacchioni, A. Selloni, S. Livraghi, E. Giamello, J. Phys. Chem. B 109 (2005) 11414.
[24] G.R. Toores, T. Lindgren, J. Lu, C.-G. Granqvist, S.-E. Lindquist, J. Phys. Chem. B 109 (2004) 5995.
[25] J.L. Gole, J.D. Stout, J. Phys. Chem. B 108 (2004) 1230.
[26] S. Sakthivel, M. Janczarek, H. Kisch, J. Phys. Chem. B 108 (2004) 1230.
[27] A. Kasahara, K. Nukumizu, T. Takata, J. Kondo, M. Hara, H. Kobayashi, K. Domen, J. Phys. Chem. B 107 (2003) 791.
[28] Y. He, Y. Zhu, Chem. Lett. 33 (2004) 900.
[29] T. Ishihara, N. Baik, N. Ono, H. Nishiguchi, Y. Takita, J. Photochem. Photobio. A 167 (2004) 149.
[30] H. Fu, C. Pan, W. Yao, Y. Zhu, J. Phys. Chem. B 109 (2005) 22432.
[31] C. Zhang, Y. Zhu, Chem. Mater. 17 (2005) 3537.
[32] H. Fu, L. Zhang, S. Zhang, Y. Zhu, J. Phys. Chem. B 110 (2006) 3061.
[33] S. Yu, B. Liu, M. Mo, J. Huang, X. Liu, Y. Qian, Adv. Funct. Mater. 13 (2003) 639.
[34] N. Masaki, S. Uchida, H. Yamane, T. Sato, Chem. Mater. 14 (2002) 419.
[35] M.A. Butler, Appl. Phys. 48 (1977) 914.
[36] M. Yoshino, M. Kakihana, W. Cho, H. Kato, A. Kudo, Chem. Mater. 14 (2002) 3369.
[37] J. Yu, W. Ho, J. Yu, H. Yip, P. Wong, J. Zhao, Environ. Sci. Technol. 39 (2005) 1175.